Proceedings of the 16th European VLBI Network Symposium
Ros, E., Benke, P., Dzib, S., Rottmann, I., & Zensus, J.A. (eds.)
September 2nd-6th 2024, Bonn, Germany

Beyond the Core: Unveiling Multiple Gamma-Ray Production Zones in Blazar 3C 454.3

Eva Palafox[1,2],[⋆], Víctor M. Patiño-Álvarez[1,2], Vahram Chavushyan[1], Sergio A. Dzib[2], Andrei P. Lobanov[2], and J. Anton Zensus[2]

[1] Instituto Nacional de Astrofísica, Óptica y Electrónica, Luis Enrique Erro #1, Tonantzintla, Puebla 72840, México
[2] Max-Planck-Institute für Radioastronomie, Auf dem Hügel 69, D-53121 Bonn, Germany

Abstract. We present a multi-wavelength analysis of the gamma-ray emission mechanisms within blazar 3C 454.3. Using 12 years of gamma-ray data alongside multi-epoch VLBA observations at 15 and 43 GHz, we explore the correlation between the flux variability in jet features and gamma-ray activity. Our analysis reveals a significant correlation between gamma-ray flux and core emission at 43 GHz and 15 GHz, suggesting these core regions contribute substantially (37% and 30%, respectively) to the overall gamma-ray production. Furthermore, a quasi-stationary 43 GHz component at 4.6 pc and a mobile 43 GHz feature (0.8-2.3 pc, $\beta_{\rm app} = 9.9 \pm 1.1$) exhibit strong correlations with gamma-ray variations, contributing 18% and 26% to the high-energy emission, respectively. The observed co-variability across these extended jet regions strongly suggests Synchrotron Self-Compton (SSC) as the primary gamma-ray production mechanism. Our discovery of a high-speed component contributing to gamma-ray emission significantly challenges existing theoretical models. Our findings highlight the potential presence of multiple, and potentially non-stationary, gamma-ray emitting regions within blazar jets, furthering our understanding of blazar complexity and SSC processes.

1. Introduction

3C 454.3 is one of the brightest sources in the $\gamma-$ray sky. Between 2009 and 2010, it presented a series of important $\gamma-$ray flares (Vercellone et al. 2011). The late-2010 flare stands out as the brightest ever recorded at the time, reaching a peak flux of $F = (8.5 \pm 0.5) \times 10^{-5}$photons cm^{-2}s^{-1} (Abdo et al. 2011). This translates to an isotropic luminosity of approximately 10^{50}erg s^{-1} (Sahakyan 2021), solidifying its place among the brightest $\gamma-$ray sources known.

Extensive research has confirmed a strong correlation between the $\gamma-$ray variability and radio frequencies, as well as other wavelengths (e.g., Jorstad et al. 2010, León-Tavares et al. 2013, Liodakis et al. 2020, Amaya-Almazán et al. 2021, Paraschos et al. 2023). The passage of a plasma component down the jet is believed to be a primary driver for most $\gamma-$ray flares (e.g., Marscher et al. 2010). In some cases, the flares coincide with the interaction of superluminal components within the jet, such as their passage through a quasi-stationary feature or the core (e.g., Agudo et al. 2011, Liodakis et al. 2020). For instance, Jorstad et al. (2013) proposed that the 2009-2010 flares in 3C 454.3 might be linked to the emergence and propagation of two knots within the jet, designated K09 and K10, as identified through analysis of monthly Very Long Baseline Array (VLBA) images. Correlated variability between different wavelengths can help us locate the $\gamma-$ray emission region within the jet. However, Very Long Baseline Interferometry (VLBI) offers an even more powerful tool. VLBI observations at millimeter and radio wavelengths achieve the highest spatial resolution, allowing us to pinpoint the exact location, or "blazar region", where $\gamma-$rays are produced (see review by Boccardi et al. 2017).

2. Observations and analysis

We have used $\gamma-$ray data for 3C 454.3 from the Fermi Large Area Telescope (Fermi-LAT) public archive Abdo et al. (2010). To account for the possibility of rapid $\gamma-$ray variations reported in previous studies (e.g., Pittori et al. 2018), we implemented an adaptive time binning approach. We calculated the $\gamma-$ray fluxes within time bins centered on the specific dates when VLBA observations were made. The bin sizes were iteratively increased, starting small and always maintaining the VLBA observation date as the center. This process continued until the test statistic (TS) for each bin exceeded a threshold of 25.

We used 137 VLBA maps at 43 GHz (7 mm wavelength) from the Boston University VLBA Blazar monitoring programs, between 2008 and 2020[1]. The program details, observations, and data reduction are described in Jorstad et al. (2017). Additionally, we included 54 images at 15 GHz from the MOJAVE program,

[⋆] eva.palafox@gmail.com

[1] http://www.bu.edu/blazars/BEAM-ME.html

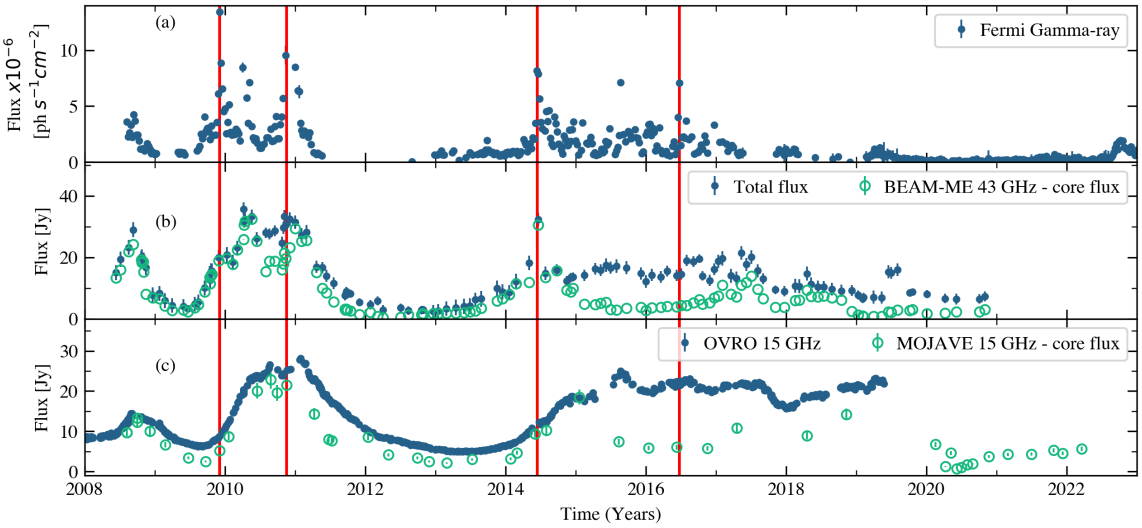

Fig. 1. Multi-wavelength light curves of 3C 454.3. Each panel shows the blazar emission at a different wavelength (indicated by the label and color). Data source is specified within each panel. Red vertical lines mark $\gamma-$ray flare events that appear to coincide with the passage of a jet component through the core.

(Lister et al. 2018)[2]. The images were taken from mid-2008 to late 2021[3].

To characterize the pc-scale jet structure from the VLBA images we used the CASA task `IMFIT` to model the emission of each component, including the core, fitting 2D elliptical Gaussian components. We considered a model feature detected if its flux exceeded a 6σ threshold from the background emission. For both frequencies, we identified the core as the easternmost component, along with other relevant knots in each map. Each component was cross-identified between different epochs by comparing the integrated flux and position relative to the core. The jet components, or knots, were named according to the frequency at which they were observed (Q for 43 GHz and K for 15 GHz). Components identified in fewer than 5 epochs were omitted. For comparison, we present the light curve of the total 43 GHz flux in Fig. 1, panel (b), alongside the core light curve at the same frequency. The core light curve for the 15 GHz VLBA maps is shown in panel (c) of the same figure, along with the total flux at 15 GHz obtained from OVRO single-dish data.

The observations made using high angular resolution VLBA have revealed that 3C 454.3 can be categorized as core-dominated between 2008 and 2020, with a few exceptional time intervals where the flux is dominated by some other component, displaying an intricate multi-component jet structure. We also tracked the temporal evolution of the radial separation between the different jet components and the radio core between 2008 and 2020, enabling the calculation of their proper motions and apparent velocities (see Fig 2).

[2] `https://www.cv.nrao.edu/MOJAVE/project.html`

[3] However, data from 2019 was excluded due to a known systematic: `https://science.nrao.edu/enews/14.4/index.shtml#vlba_flux`.

3. Results

3.1. Jet Structure and Kinematics

In our analysis of the VLBA maps at 43 GHz we characterized the core (Q0), assumed to be a stationary element situated at the eastern end of the jet, along with several other notable features. We observed a quasi-stationary component oscillating between 0.5 and 0.6 mas, which was visible during two different time intervals: Q8 between 2011 and 2014, and Q21 from 2016 to 2020. This component was previously observed and labeled St (e.g. Jorstad et al. 2005, 2013) or region C (e.g. Traianou et al. 2024). Additionally, we identified 20 moving components labeled Q1, Q2, and so on, up to Q24 (excluding Q8 and Q21, as already mentioned). Most of the modeled components are consistent with knots discussed in earlier studies. For instance, Q3 was ejected from the core in early 2010, corresponding with the time of the $\gamma-$ray flare observed between September 2009 and January 2010. This component was previously identified as K09, as reported by Jorstad et al. (2013), and its passage through the core was associated with a multi-wavelength outburst in 3C 454.3. Similarly, Q10, Q17, Q19, and Q18 seemed to align with the knots referenced by Traianou et al. 2024 as the disappearing knots observed at 43 and 86 GHz. These four components seemed to vanish once they approached the quasi-stationary component Q21 (or region C in their study), as depicted in Fig. 2. They proposed that this disappearance might be attributed to the bending of the jet at that specific location, causing the plasma to shift toward the observer line of sight. The model fitting of VLBI maps at 15 GHz reveals a complex jet structure oriented towards the northwest, exhibiting subtle variations over time. This finding is further supported by observations from August 2008

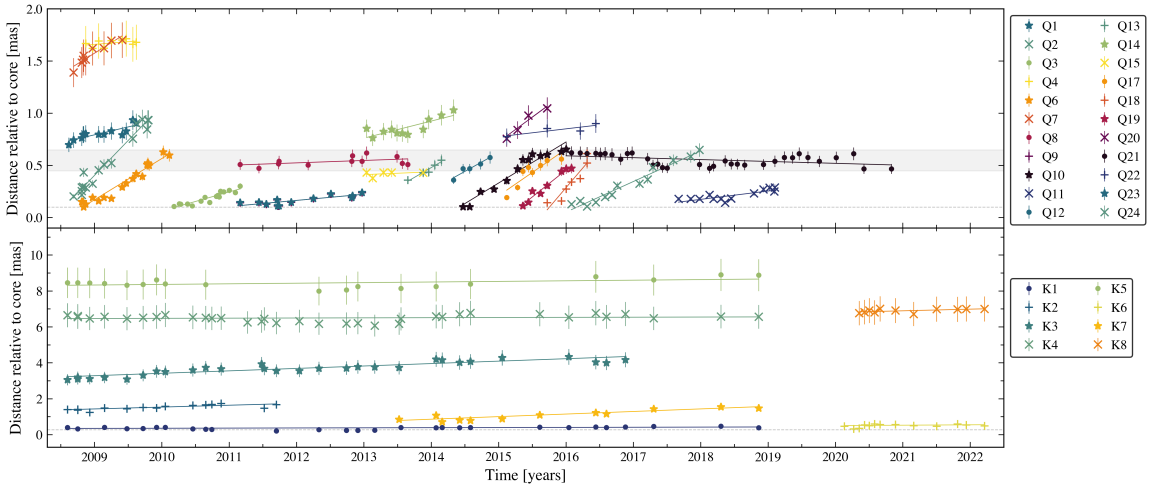

Fig. 2. Relative distance to the core versus time of all the identified jet components in 3C 454.3 at 43 (upper panel) and 15 GHz (lower panel). The gray shadowed area represents the position of the quasi-stationary region (ST) reported by this and previous studies. The dashed horizontal line shows the typical angular resolution.

Table 1. Kinematic parameters of the identified jet components in the VLBA maps at 43 GHz.

ID	t_{eject} (yr)	μ (mas yr^{-1})	$\beta_{\rm app}$ (c)	$d_{\rm core}$ (pc)
Q3	2009.7	0.21±0.02	9.9±1.1	–
Q21	–	-0.02±0.03	–	4.28±0.13
K6	1997.8	0.22±0.25	–	3.9±0.1.
K8	–	0.09±0.09	–	53.18±0.01

Columns from left to right: (1) component ID, (2) estimation of the time in which it was ejected from the core, (3) proper motions, (4) apparent speed, and (4) projected distance to the core in pc.

to the end of 2020, which consistently depict the source as core-dominated with a persistent one-sided jet. The brightest component, designated K0, is followed by K1, a quasi-stationary jet feature located on average 0.4 mas away from the core. Notably, K1 remained attached to the core from mid-2008 to 2013. By the end of 2020, a new component, K6, emerged. K6 originated from K1 initial position and moved away from K0, potentially linked to the $\gamma-$ray emission, as discussed later. Given that we excluded the 15 GHz VLBA 2019 data from our analysis, we cannot definitively confirm if K6 originated from the same K1 component observed earlier. In addition to the moving components and the core, we identified two other quasi-stationary features, K4 and K5, located at approximately 6.5 mas and 8.5 mas from the core, respectively.

We calculated the apparent speed ($\beta_{\rm app}$) of the moving components following the relationship

$$\beta_{\rm app} = \frac{\mu D_L}{c(1+z)} \quad (1)$$

where μ is the proper motion in rad s^{-1}, D_L is the luminosity distance in m, z is the source redshift, and c is the speed of light in m s^{-1}.

3.2. Correlation Analysis

The connection between the $\gamma-$ray state of blazars and their parsec-scale jet behavior is well established. Studies by León-Tavares et al. (2011) suggest that the brightest $\gamma-$ray flares in blazars might be triggered by the initial stages of millimeter-wavelength outbursts. To quantify the potential link between the variability of the parsec-scale jet knots in 3C 454.3 and its $\gamma-$ray emission, we performed Spearman rank correlation tests. We consider a given correlation as significant if the probability of obtaining a specific correlation coefficient due to statistical fluctuations has p-value < 0.05. This approach ensures we capture potential correlations while maintaining the temporal resolution necessary to detect rapid variability. The

Table 2. Spearman rank correlation coefficients.

ID	ρ	ρ^2	p-value
Q0	0.52	0.27	2.4×10^{-9}
Q3	0.53	0.28	0.01
Q21	0.45	0.20	0.01
K0	0.62	0.39	1×10^{-5}
K6	-0.65	0.42	0.02
K8	-0.64	0.40	0.04

Columns from left to right: (1) component ID, (2) Spearman rank correlation coefficient, (3) correlation coefficient squared, (4) p-value.

results of our analysis are presented in Table 2, they reveal that both 43 GHz and 15 GHz core emissions strongly correlate with $\gamma-$ray emission. The 43 GHz core has a

correlation coefficient of 0.52. This indicates that approximately 27% of the variability in $\gamma-$ray emission is related to the variability in the core radio emission. Similarly, the flux of the 15 GHz core contributes approximately 40% to the high-energy emission.

The quasi-stationary component Q21 in the 43 GHz maps, visible between 2016 and 2021, at a projected distance of 4.6 pc (0.6 mas), strongly correlates with the $\gamma-$ray flux. This component accounts for 18% of the high-energy emission. The quasi-stationary component, which also corresponds to Q8, does not correlate all the time, which indicates that it is not an important source of $\gamma-$rays all the time. We also detected a mobile component whose flux exhibits a robust correlation with the $\gamma-$ray flux, contributing to 26% of the high-energy emission between 2010.18 and 2011.16. This component denoted as Q3, demonstrates an apparent velocity of $\beta_{\rm app} = 9.9 \pm 1.1$ c, observed at a projected distance ranging from 0.8 to 2.3 pc (0.1 to 0.3 mas). For $\gamma-$ray emission regions located farther than one pc from the central BH (e.g., components Q21 and Q3), our findings suggest synchrotron self-Compton (SSC) as the primary mechanism responsible for the high-energy radiation.

Interestingly, a new jet component, K6, emerged near the end of the study period (early 2020). This component shows a significant anti-correlation with the $\gamma-$ray flux, with a coefficient of -0.65, suggesting that nearly 40% of the $\gamma-$ray variability during this specific time might be related to the ejection and 15 GHz emission of K6, even in the absence of a simultaneous flare. As suggested by Patiño-Álvarez et al. (2018), one possible explanation for the observed behavior is that the jet has become less transparent to $\gamma-$rays. The cross-section for both the inverse Compton scattering and the triple pair production are dependent on the energy of the electrons in the jet, when the Lorentz factors of individual electrons increase up to a certain threshold, the triple pair production cross-section becomes more prominent than the inverse Compton. This process would absorb $\gamma-$rays, causing a flux decrease, while at the same time, increasing the synchrotron emission, due to the increase in the Lorentz factor, and the production of more leptons within the jet. However, K6 proximity to the core, near the spatial resolution limit, raises the possibility of flux contamination. Additionally, a quasi-stationary component, K8, was detected at roughly 53 pc from the core. While correlation analysis was feasible with 11 epochs, further observations are essential to ascertain this relationship.

4. Summary

This study reveal the presence of multiple distinct regions within the jet that contribute to the high-energy emission. Intriguingly, some of these emission regions appear to be non-stationary, exhibiting variations over time. Furthermore, we were able to pinpoint the exact locations of these regions within the blazar jet itself. For non-core components (i.e., those located farther from the central pc), the correlation observed in simultaneous data suggests that the $\gamma-$ray emission mechanism is synchrotron self-Compton. These findings could guide the development of more comprehensive theoretical models that might account for the observed variability and spatial distribution of high-energy emissions.

Acknowledgements. This research makes use of VLBA data from the VLBA-BU Blazar Monitoring Program (BEAM-ME and VLBA-BU-BLAZAR; http://www.bu.edu/blazars/BEAM-ME.html), funded by NASA through the Fermi Guest Investigator Program. This research has made use of data from the MOJAVE database that is maintained by the MOJAVE team (Lister et al. 2018). This publication acknowledges project M2FINDERS, which is funded by the European Research Council (ERC) under the European Union's Horizon 2020 research and innovation programme (grant agreement no. 101018682). This work is supported by CONAHCyT research grants 280789 and 320987, and by the MPIfR-Mexico Max Planck Partner Group led by VMP-A.

References

Abdo, A. A., Ackermann, M., Ajello, M., et al. 2010, ApJS, 188, 405
Abdo, A. A., Ackermann, M., Ajello, M., et al. 2011, ApJ, 733, L26
Agudo, I., Marscher, A. P., Jorstad, S. G., et al. 2011, ApJ, 735, L10
Amaya-Almazán, R. A., Chavushyan, V., & Patiño-Álvarez, V. M. 2021, ApJ, 906, 5
Boccardi, B., Krichbaum, T. P., Ros, E., et al. 2017, A&A Rev., 25, 4
Hovatta, T. & Lindfors, E. 2019, New A Rev., 87, 101541
Jorstad, S. G., Marscher, A. P., Larionov, V. M., et al. 2010, ApJ, 715, 362
Jorstad, S. G., Marscher, A. P., Morozova, D. A., et al. 2017, ApJ, 846, 98
Jorstad, S. G., Marscher, A. P., Smith, P. S., et al. 2013, ApJ, 773, 147
Jorstad, S. G., Marscher, A. P., Lister, M. L., et al. 2005, AJ, 130, 1418
León-Tavares, J., Chavushyan, V., Patiño-Álvarez, V., et al. 2013, ApJ, 763, L36
León-Tavares, J., Valtaoja, E., Tornikoski, M., et al. 2011, A&A, 532, A146
Liodakis, I., Blinov, D., Jorstad, S. G., et al. 2020, ApJ, 902, 61
Lister, M. L., Aller, M. F., Aller, H. D., et al. 2018, ApJS, 234, 12
Marscher, A. P., Jorstad, S. G., Larionov, V. M., et al. 2010, ApJ, 710, L126
Paraschos, G. F., Mpisketzis, V., Kim, J.-Y., et al. 2023, A&A, 669, A32
Patiño-Álvarez, V. M., Fernandes, S., Chavushyan, V., et al. 2018, MNRAS, 479, 2037
Pittori, C., Lucarelli, F., Verrecchia, F., et al. 2018, ApJ, 856, 99
Sahakyan, N. 2021, MNRAS, 504, 5074
Traianou, E., Krichbaum, T. P., Gómez, J. L., et al. 2024, A&A, 682, A154
Vercellone, S., Striani, E., Vittorini, V., et al. 2011, ApJ, 736, L38